Available online at www.sciencedirect.com

jmr&t
Journal of Materials Research and Technology

journal homepage: www.elsevier.com/locate/jmrt

Improved mechanical and wear properties of H13 tool steel by nitrogen-expanded martensite using current-controlled plasma nitriding

A.K. Gonzalez-Moran [a], M. Naeem [b], H.M. Hdz-García [a], E.E. Granda-Gutiérrez [c], J.J. Ruíz-Mondragón [a], M. Alvarez-Vera [d], J.C. Díaz-Guillén [e,*]

[a] Corporación Mexicana de Investigación en Materiales, Saltillo, Mexico
[b] Department of Physics, Women University of Azad Jammu and Kashmir, Bagh, Pakistan
[c] UAEM University Center at Atlacomulco, Universidad Autónoma Del Estado de México, Atlacomulco, Mexico
[d] Universidad de Las Américas Puebla, UDLA, Dpto. de Ingeniería Industrial y Mecánica, Cholula, Mexico
[e] CONACYT- Corporación Mexicana de Investigación en Materiales, Saltillo, Mexico

ARTICLE INFO

Article history:
Received 24 April 2023
Accepted 23 June 2023
Available online 26 June 2023

Keywords:
Plasma nitriding
Expanded martensite
Wear
Elastic properties

ABSTRACT

Nitrogen-expanded martensite is a crystalline structure formed by incorporating nitrogen atoms into the interstitial sites of martensitic steels. It has recently gained significant industrial attention due to its excellent mechanical and wear-resistance properties. However, the major challenge in synthesizing nitrogen-expanded martensite is obtaining a phase free of iron or chromium nitrides precipitates. In this study, the effects of varying temperature (460, 480, and 500 °C) and plasma current density (0.5, 1.0, and 1.5 mA/cm^2) during plasma nitriding of H13 tool steel were investigated to evaluate their influence on crystalline phases. The results of X-ray diffraction analysis indicate that expanded martensite free of nitride precipitates can be obtained at a temperature of 480 °C and low current density. Moreover, wear analysis using a ball-on-disk wear tester showed that the lowest wear rates were achieved under similar conditions. Grazing incidence X-ray diffraction analysis revealed that the outer region of the nitrided zone had a disordered structure, which could be attributed to a nano crystallization process. The nanoindentation analysis demonstrated that the expanded martensite phase has rigid-elastic properties characterized by high elastic energy (144.5 nJ) and high resistance to plastic deformation.

1. Introduction

The demand for high-performance metallic alloys in various technological applications has driven the development of new materials and the improvement of commonly used ones. Enhancing material properties enables their use in new and more demanding applications and increases their lifespan in current processes. For instance, AISI H13 alloy is a popular hot work tool steel with excellent high-temperature strength,

* Corresponding author.
E-mail address: jcarlos@comimsa.com (J.C. Díaz-Guillén).
https://doi.org/10.1016/j.jmrt.2023.06.221

toughness, ductility, and hardenability, making it suitable for die manufacturing, light-metals injection, and forging. Despite its good mechanical properties, H13 tool steel has limited tribological performance, which necessitates the replacement of components made of this alloy within a short period. Therefore, various technologies, such as hard coating or thermochemical treatments, have been employed to improve the lifespan of tool steels [1–7].

Plasma nitriding is a widely used thermochemical treatment that enhances the surface properties of steel, including hardness; wear resistance, fatigue resistance, and corrosion resistance. This process introduces atomic nitrogen into the surface and subsurface of metallic pieces, resulting in a dual-layer structure consisting of a thin nitride layer on top of a thicker diffusion zone. The formation of a thin layer (also called white or compound layer) is a challenge for the nitriding process, particularly for applications in forging or extrusion dies where serious impact and heavy wear are present [8]. This hard but brittle layer must be removed by grinding, which involves additional operations and increases processing costs. Furthermore, removing the white layer in complex shapes such as dies can be laborious or even impossible [5,9]. In this context, it is essential to investigate nitriding conditions that can prevent the formation of an undesirable white layer. It has been determined that surface characteristics of the nitrided layer and even specific surface properties can be developed by controlling the nitriding potential.

Nitriding of H13 tool steel has been shown to improve productivity and quality in various industries and extend the lifespan of critical tools made with this alloy. This surface modification treatment can enhance the fatigue, tribological, and corrosion properties of H13 steel by forming high nitrogen phases on the specimen's surface. However, it is crucial to carefully control the nitriding conditions to prevent the precipitation of CrN, which can detriment the corrosion properties of this alloy [10].

Research has been conducted on nitrogen incorporation in austenitic stainless steels with fcc structures, with a focus on preventing the precipitation of chemical compounds such as iron and chromium nitrides [11]. The result is a solid supersaturated solution with interstitial nitrogen, known as expanded austenite (S phase) which exhibits superior mechanical properties and remarkable corrosion performance, particularly in the absence of CrN precipitates [12,13]. However, there is limited literature on nitrogen saturation in bcc iron structures [14–16]. Specific processing conditions in this kind of structure result in the formation of the expanded martensite phase, characterized by its high hardness, exceptional resistance to cavitation erosion, and good wear performance [14,17–19].

Expanded martensite is a type of solid solution formed by the diffusion of nitrogen atoms into the crystal lattice of the martensite phase of steel [20,21]. This process creates a highly distorted lattice structure, which causes the XRD peaks of the expanded martensite to shift towards lower angles compared to the original martensite phase reflections [22].

Several authors have conducted investigations on the properties and formation of expanded martensite under different nitriding conditions. Wang et al. [23] reported on the gas nitriding of H13 tool steel and examined the impact of nitrogen potential on microstructure, surface hardness, and wear resistance. They discovered that both the hardness and thickness of the nitrided layer increase with higher nitrogen potential. The nitrided samples with a compound layer (white layer) demonstrated excellent wear resistance under light loads, while the compound-free diffusion zone exhibited exceptional wear resistance under heavy loads. Fazel et al. [24] focused on studying the effect of the white layer on the corrosion resistance of plasma-nitrided H13 tool steel in a 3.5% NaCl solution. They observed that removing the white layer from the nitrided tool steel had a positive effect on corrosion resistance. Peng et al. [25] compared the service life and stamping ability of plasma-nitrided H13 tool steel with and without a white layer by varying the processing temperature; they reported that the service life of working dies increased up to 10 times when using non-compound layer plasma nitriding. In a separate study, Fernandes et al. [7] varied the plasma nitriding temperature of H13 tool steel and found that low-temperature nitriding (450 °C) only resulted in a diffusion zone, while high-temperature nitriding (550 and 650 °C) created a compound layer over the diffusion zone. Jacobsen et al. [26] reported the formation of expanded martensite with low content of $Fe_{2\text{-}3.2}N$ on H13 tool steel by plasma nitriding at 430 °C for 5 h, using a current density of 8.8 mA/cm^2. They suggested that the plasma current density and processing temperature work together to form the expanded martensite phase. They also reported a significant reduction in wear rate of up to 8–10 times for the nitrided samples. Miyamoto et al. [5] informed that expanded martensite formation without forming a compound layer is possible in the nitriding of H13 tool steel with neutral nitrogen species. In a previous study [6], we observed expanded martensite formation on H13 steel by pulsed plasma nitriding and the presence of the Fe_3N phase as a remnant of the white layer. The nitrided samples showed a 26% reduction in volume loss compared to untreated material, with a slightly lower friction coefficient observed for the expanded martensite phase.

Overall, expanded martensite has been found to have improved mechanical properties such as wear resistance and elastic response compared to untreated steel. Nitriding conditions can influence its properties, and researchers continue investigating its formation and properties.

The plasma current density is a critical parameter in plasma nitriding, and it plays a crucial role in determining the properties of the nitrided steel. However, limited information is available in the literature on the effects of plasma current density on the nitriding response [26]. Previously, Jacobsen et al. [26] investigated the influence of current density on the phase structure and tribological properties of nitrided H13 tool steel. They achieved different current densities by altering the metallic shield under the sample holder, thereby varying the electrode area. In this study, we investigate the effect of current density by modifying the current generated by the power supply while keeping the electrode area constant. This approach ensures consistent electrodes and avoids the possibility of significant fluctuations in current density. Furthermore, controlling the plasma current density can modify the quantity of nitrogen ions in

the plasma and consequently, the chemical composition of the nitrided steel. Thus, the present study investigates the effect of plasma current density and sample temperature on the surface properties of plasma nitrided H13 tool steel. By varying the plasma current density and sample temperature, it could be explained how these parameters affect the nitriding response and how the resulting changes in nitrogen ion density and chemical composition affect the surface properties of the steel. This study is also helpful for understanding the fundamental mechanisms behind plasma nitriding and optimizing the process parameters to achieve desired surface properties in H13 tool steel.

2. Methods

The AISI H13 tool steel disk-shaped samples used in the study (38.1 mm in diameter, 4 mm in height) were cut from a commercial rod with a chemical composition of (wt. %) 0.38C, 0.30Mn, 0.90Si, 5.5Cr, 1.2Mo, 0.80 V and Fe balance. To prepare the samples for nitriding, they were heat treated in a furnace at austenitizing temperature of 1020 °C for 25 min and then air-quenched. A double tempering process was then applied at 540 °C for 120 min, resulting in a hardness value of 50 HRC. To ensure a smooth surface finish, the samples were polished with emery paper of grit 80–1200; also, diamond paste was used as an abrasive media, resulting in a surface roughness (Ra) of 0.02 μm. Finally, the samples were subjected to ultrasonic cleaning in acetone to remove any residual polishing debris or contaminants. This preparation process is important to ensure consistent and reproducible results in the nitriding treatment.

Subsequently, plasma nitriding was performed in a laboratory reactor using a constant direct current (DC) plasma produced in a gas mixture of 50% N_2 and 50% H_2 at 266 Pa (1.3 Pa base pressure). The samples under treatment formed the cathode, while the cylindrical stainless-steel reactor was used as the anode. The study parameters were sample temperature and plasma current density, and each sample was labeled and treated according to conditions listed in Table 1. An insulated auxiliary heating system was placed beneath the sample holder to heat the samples. The treatment temperature was regulated by an electronic controller and a type K thermocouple attached to a dummy sample. The plasma current densities were calculated based on the electrical current provided by the power supply and the total area of the cathode exposed to the plasma (the samples). Current value was set constant, allowing a free bias potential adjustment, which average values were 428 V, 500 V and 520 V for current densities of 0.5 mA/cm^2, 1.0 mA/cm^2 and 1.5 mA/cm^2 respectively. After 4 h of nitriding, the plasma and heating systems were turned off, and the samples were cooled to room temperature inside the reactor, which was filled with an inert argon atmosphere.

The chemical and morphological changes on the surface and cross sections of nitrided samples were analyzed using a Tescan Mira 3 Field Emission Scanning Electron Microscopy (FE-SEM) equipped with Energy Dispersive Spectroscopy (EDS) detector. X-ray diffraction (XRD) analysis was performed in conventional and grazing incidence (GIXRD) modes to identify the phase composition. A Malvern Panalytical Empyrean X-ray diffractometer was used for standard mode analysis, which employed 45kV-40mA Cu-Kα radiation in a 2θ range of 37–70° (with an analysis time of 14 s per step and a resolution of 0.013°). To determine possible structural variations in the depth of the nitrided surfaces, the main XRD reflection (110) for expanded martensite was scanned by GIXRD from 42 to 46° 2θ at incidence angles (ω) of 0.3, 0.5, 1.0, and 1.5°. The average crystallite size was also determined from the (110) expanded martensite reflections using the Scherrer equation [27].

Vickers surface hardness of untreated and nitrided samples was measured using a Buehler Micromet 5103 micro durometer. It is reported the average of 8 measurements carried on samples surface using 200 g load during 15 s. The wear performance of untreated and nitrided samples was assessed by conducting dry ball-on-disk method using an alumina ball following the procedure of ASTM G99-17 standard [28]. The parameters of ball-on-disk test of untreated and nitrided samples are showed in Table 2. By the use of an optical profilometer (Keyence VR-6000), wear tracks profiles were measured and track cross area was obtained. The wear volume was calculated by multiplying track cross area by the perimeter of the track. Furthermore, the specific wear rate coefficient was determined using the Archard model: $V = kFs$, where V is the wear volume (mm^3), F is the normal load (N), s is the sliding distance (m) and k is the specific wear rate coefficient (mm^3/Nm) [29].

Micromechanical characterization was performed using a Rtec Nanoindentation tester, with a maximum load of 250 μN. Nano hardness (H), elastic moduli (E), as well as plastic (W_p) and elastic (W_e) energy were determined. To evaluate the plastic and elastic performance, micromechanical rates ($H/E, H/E^2, H^3/E^2$) were also calculated.

Table 1 – Experimental conditions and samples identification.

Sample identification	Temperature (°C)	Current Density (mA/cm^2)
N460–0.5	460	0.5
N460–1.0		1.0
N460–1.5		1.5
N480–0.5	480	0.5
N480–1.0		1.0
N480–1.5		1.5
N500–0.5	500	0.5
N500–1.0		1.0
N500–1.5		1.5

Table 2 – Test Parameters used for ball-on-disk tests.

Normal Force (N)	4
Sliding Distance (m)	330
Sliding Speed (m/s)	0.1
Pin-end Diameter, spherical (mm)	6
Environment	air
Nominal Temperature (°C)	23
Track Diameter (mm)	7

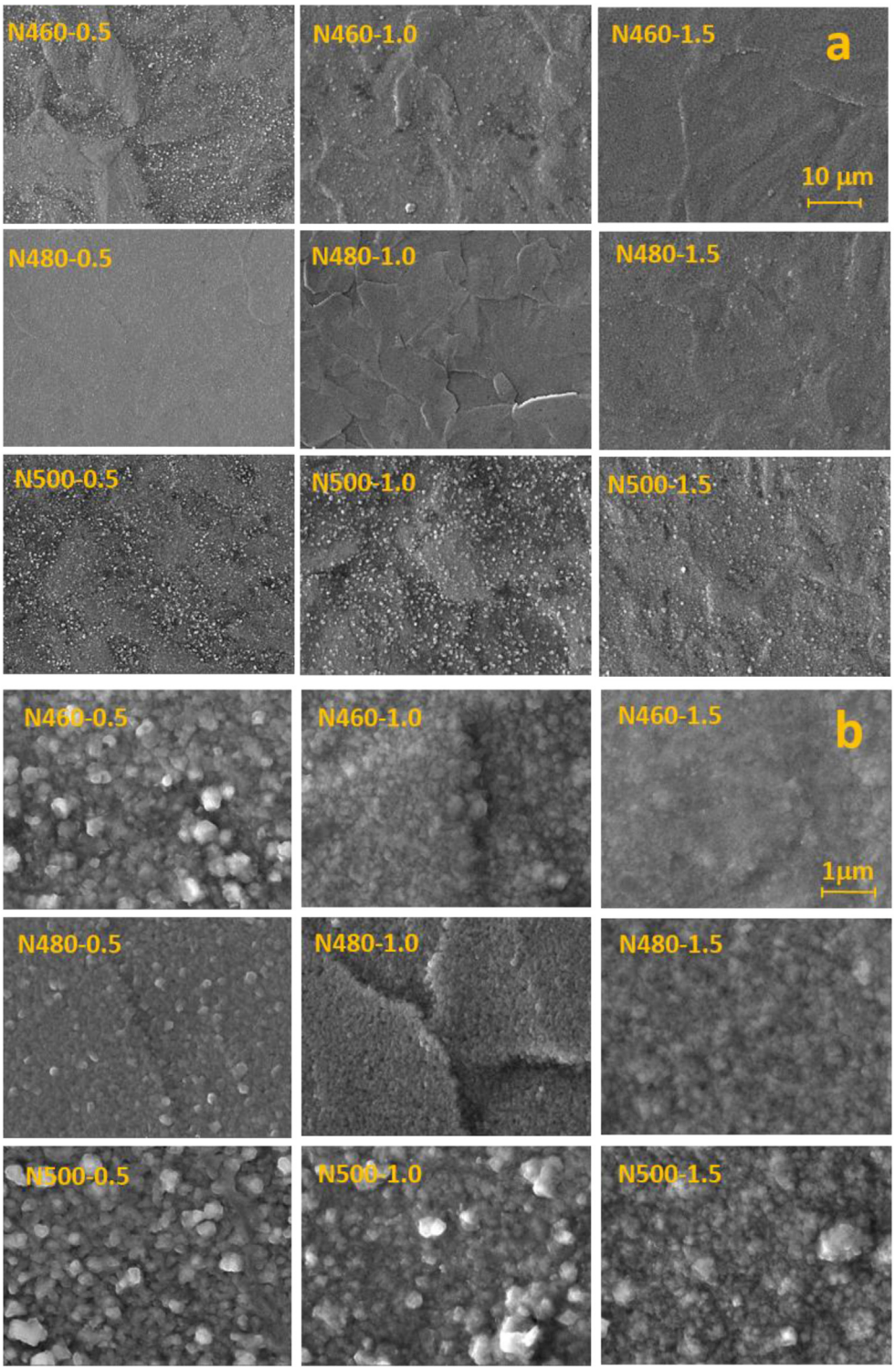

Fig. 1 – (a) Low and (b) high magnification micrographs of H13 tool steel samples plasma nitrided at different conditions.

3. Results and discussion

3.1. *Nitrided samples characterization*

SEM micrographs of nitrided samples under different conditions are presented in Fig. 1(a) and (b), showing low and high-magnification surface views, respectively. All samples exhibit grain boundaries revealed due to the plasma ions sputtering and strain phenomena. Nitrogen incorporation induces compressive residual stresses that can cause heterogeneous structural deformation and potentially lead to microstructural changes [18]. In samples treated at 460 °C and 500 °C, agglomerated particles are deposited on the surfaces, while samples treated at 480 °C exhibit surfaces with very few or no

Table 3 – EDS chemical analysis on agglomerated particles.

Element	Fe	O	N	Cr	Si	Mo
Weight %	80.82	7.25	4.75	5.11	1.0	1.08

agglomerated particles. The metallic particles in plasma generated by the sputtering process (produced by the ions impinging the sample surface) react with nitrogen ions near the sample surface; then, they are re-deposited on it, resulting in the formation of agglomerated particle morphology [30]. The sputtering rate varies with the plasma density, which is affected by processing conditions such as pressure, temperature, and gas mixture [31]. Thus, samples treated at 480 °C (with 0.5 and 1.0 mA/cm^2 current density) show a smoother surfaces with no agglomerated particle formation, likely due to the lower impingement energy of nitrogen ions on the sample surface at this temperature and current densities. Table 3 presents the average EDS chemical composition of several agglomerated particles on the surface of the samples. The results indicate that residual oxygen in the plasma, caused by the rough vacuum conditions employed in these processes, reacts with the sputtered particles, leading to the formation of oxides that are incorporated into these agglomerated particles [32] (See. Table 4).

The plasma interactions with the surface of samples can cause variations in surface roughness, as described above. Fig. 2 (a) illustrates how the current density and temperature influence the roughness of all samples. The highest roughness values were obtained for samples treated at 460 °C and 500 °C using current densities of 0.5 and 1.0 mA/cm^2. At a current density of 1.5 mA/cm^2, the temperature has a minor effect on roughness, and similar values are obtained for all evaluated temperatures. Samples N480–0.5 and N480–1.0 showed the lowest roughness values, indicating less impact of sputtering and re-deposition phenomena. A proportional relationship between roughness and current density can also be observed at 480 °C.

During plasma nitriding, the process temperature plays an essential role in the diffusion mechanisms and the sputtering phenomena [33]. Excitation, ionization, and elastic collisions between electrons and molecules and elastic collisions of fast atoms with slow atoms are most important in the nitriding reaction and are affected by surface and plasma temperature [34]. Then, the different behavior of surface roughness observed in Fig. 2 could be mainly associated with the temperature because this parameter influences the production of nitrogen and nitrogen-hydrogen species as the active plasma components. The relative concentration of these species exhibit non-linear trends in relation to the temperature and is also affected by other parameters, including pressure, plasma polarization potential, surface composition, and others [33,35]. Consequently, for this research study, we propose to evaluate the resulting surface roughness for individual values of temperatures only.

The trend for atomic nitrogen content on the surface of treated samples is similar, as shown in Fig. 2 (b). Nitrogen content was determined using the EDS technique, averaging several semi-quantitative nitrogen values. An increase in current density leads to higher nitrogen contents on the surface, with the highest content (approximately 20 at. %) observed at a current density of 1.5 mA/cm^2, regardless of the temperature. In contrast, an increase in temperature results in a decrease in nitrogen content. This can be attributed to the prevalence of lower nitrogen content phases (as Fe_4N) at higher temperatures, as was also reported by Jacobsen et al. [26].

The XRD pattern for H13 tool steel is shown in Fig. 3. It reveals main reflections from the α-Fe phase located at 44.47° and 64.64°, which are oriented in (110) and (200) planes, respectively, with a body-centered cubic structure (ICDD 04-002-1833).

Fig. 4 depicts the XRD spectra of nitrided samples subjected to different processing conditions. At a nitriding temperature of 460 °C, the modified layer is composed of expanded martensite (α_N) whose reflection is shifted to a lower angle (43.45°) relative to the original martensite reflection (44.47°) and ε-Fe_3N nitride. Lower intensity reflections for γ′-Fe_4N are also detected at 40.89°, with intensity decreasing when the current density increases from 0.5 to 1.5 mA/cm^2. At 500 °C, a crystalline phase mixture comprising α_N, ε-Fe_3N, and γ′-Fe_4N is formed. High-intensity reflections for expanded martensite and γ′-Fe_4N are observed in the sample treated at 500 °C and 0.5 mA/cm^2. The intensity of α_N does not significantly vary with current density, while that of γ′-Fe_4N decreases as the current density increases from 0.5 to 1.5 mA/cm^2. Conversely, the intensity of ε-Fe_3N at 38.39° increases, reaching its maximum value at 1.5 mA/cm^2. The increase in ε-Fe_3N reflection intensity (phase with a higher nitrogen content) with current density at 460 °C and 500 °C can be attributed to the nitrogen potential. Higher plasma ion density is generated at higher current densities [36], making more nitrogen ions available near the sample surface during the thermal diffusion process, thus favoring the entrance of nitrogen into the metallic crystalline structure.

When samples are treated at 480 °C with current densities of 0.5 and 1.0 mA/cm^2, they result in a monophasic layer of α_N. However, a multiphase layer is generated when the current density increases to 1.5 mA/cm^2. This layer has XRD reflections similar to the sample treated at 460 °C and 500 °C with a current density of 1.5 mA/cm^2, showing a high-intensity ε-Fe_3N reflection and minor peaks of γ′-Fe_4N. For

Table 4 – Mechanical characteristics and H/E ratios obtained from nanoindentation tests.

Sample ID	E (GPa)	H (GPa)	H/E	H/E^2 (GPa^{-1})	H^3/E^2 (GPa)	W_p (nJ)	W_e (nJ)	k (mm^3/Nm 10^{-5})
H13	81.3	2.6	0.032	0.00039	0.0027	133.2	40.6	15
N480-0.5	24.2	3.4	0.140	0.00580	0.0671	49.7	144.5	0.96
N480-1.0	95.8	5.8	0.060	0.00063	0.0212	74.7	52.9	1.42
N480-1.5	148.3	16.7	0.112	0.00076	0.2117	16.2	60.2	2.8

the samples 480–0.5 and 480–1.0, the α_N (110) peaks are at 43.97° and 43.47°, respectively. These peaks are shifted by 0.5° and 1.0°, respectively, compared to the untreated sample. The magnitude of the shift of the (110) reflection follows the same trend as the nitrogen content in the nitrided samples. Higher nitrogen content results in a higher shift of the (110) reflection, which indicates a more significant expansion of the martensite reticular network due to nitrogen incorporation. Although the processing temperature is the same for both samples, variations in the current density can modify the number of nitrogen ions around the sample and, consequently, the chemical gradient. This can stimulate or limit the nitrogen diffusion process.

To verify the presence or absence of a white layer, the treated samples underwent cross-sectional scanning electron microscope analysis. Samples that exhibited the identification of ε-Fe_3N and γ′-Fe_4N also showed the presence of a white layer, which was metallographically identified as a non-chemically etched surface zone. Conversely, no white layer was observed for samples where only the displacement of the X-ray diffraction reflections of the martensite towards lower angles occurred. Fig. 5 provides representative cross-sectional SEM images, demonstrating a) the absence of a white layer (N480–0.5) and b) the presence of a white layer (N500–1.5).

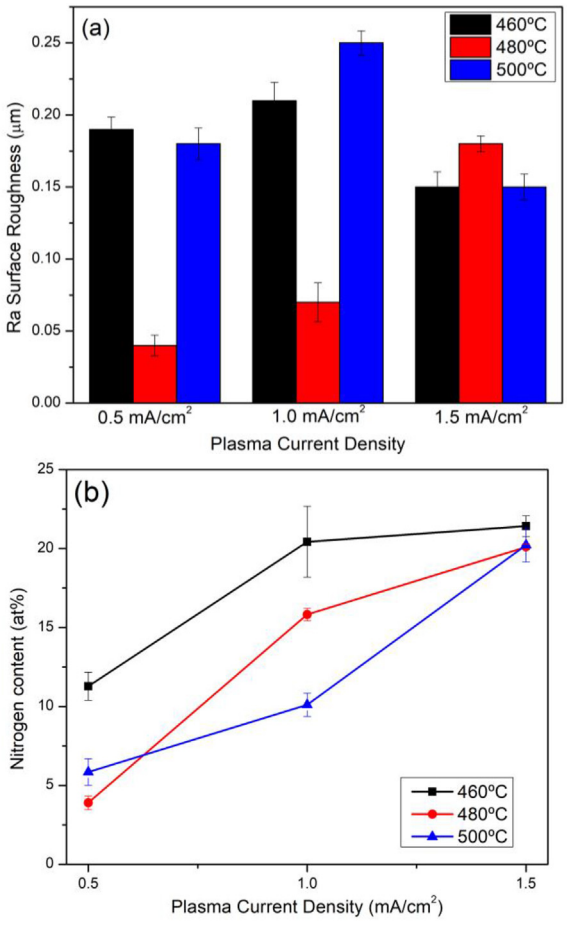

Fig. 2 – Influence of plasma current density and processing temperature on a) surface roughness and b) surface nitrogen content of nitrided samples quantified by EDS.

The cross-metallographic analysis of the treated samples revealed noticeable microstructural variations in the nitrided regions compared to the H13 substrate. Fig. 6a displays a micrograph of untreated H13 steel (after etching with Nital 5%), exhibiting the typical martensite matrix with a high martensite content, the presence of carbides, and a small amount of retained austenite visible between the martensite plates. Fig. 6b, c, and d present metallographic views of the regions beneath the white layer (where applicable) for samples N460–0.5, N480–0.5, and N500–0.5, respectively. In general, the microstructure of these regions is characterized by large plates of martensite that intersect with carbides (indicated by yellow arrows), along with dispersed grains of retained austenite. The quantity of retained austenite appears to be higher than that observed in the substrate (at the current magnification). A recent study by M. Godec et al. [3] reported a slight increase in retained austenite after a nitriding treatment for nickel-rich martensitic steel. In cases where the white layer is present (Figures b and d), there are additional nitrides along the grain boundaries (indicated by white arrows). These nitrides can be identified by their typical morphology, which has previously been associated with the predominance of a grain-boundary diffusion mechanism [37,38].

Fig. 7 displays the surface microhardness values obtained for all nitrided samples. The obtained values fall within a narrow interval, ranging from 1081 HV0.2 to 1211 HV0.2, which is more than twice as high as that of the substrate. These microhardness values are consistent with previous studies that reported the presence of a multiphasic white layer (Fe_3N, Fe_4N) [6,7]. Importantly, it should be highlighted that surfaces without a white layer exhibited microhardness values that were similar to or even higher than those of samples with a white layer.

To investigate variations in the crystalline structure of expanded martensite at different depths, grazing incidence XRD analysis was performed on the N480–0.5 and N480–1.0 samples at various incidence angles. Fig. 8 depicts the α_N (110) reflection for both samples at different ω values. The broad reflections observed at low incidence angles become narrower

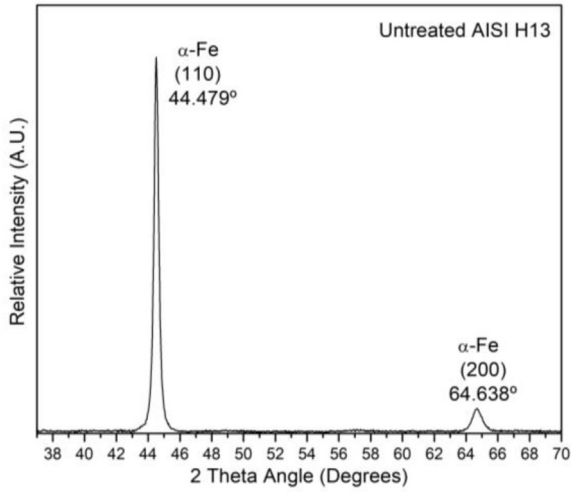

Fig. 3 – XRD pattern of untreated AISI H13 tool steel.

at higher angles. At ω = 0.3 (outer analyzed region), the 480–0.5 sample exhibits a broader and less defined reflection than the 480–1.0 sample; the latter indicates a more disordered crystalline structure in the outer region (functional section) of the nitrided area. This disordered structure could be related to a decrease in the size of diffraction coherent domains (crystallites), which can be considered a surface nanocrystallization phenomenon. The nanocrystallization effect is strongly dependent of temperature and has been associated with superior wear resistance and fatigue life [16].

The calculated crystallite size as a function of ω for both samples is also presented in Fig. 8. The results indicate a low difference in crystallite size between the two samples at ω = 0.5°, 1.0°, and 1.5°, but the difference is significant at ω = 0.3°. Hence, it is suggested that minor interstitial nitrogen incorporation in the martensite structure of the outer region of the nitrided sample (480–0.5) generates an expanded martensite phase with a short-range isotropy characteristic (nanocrystallization phenomenon). As more nitrogen is incorporated into the original martensite, the crystallinity of

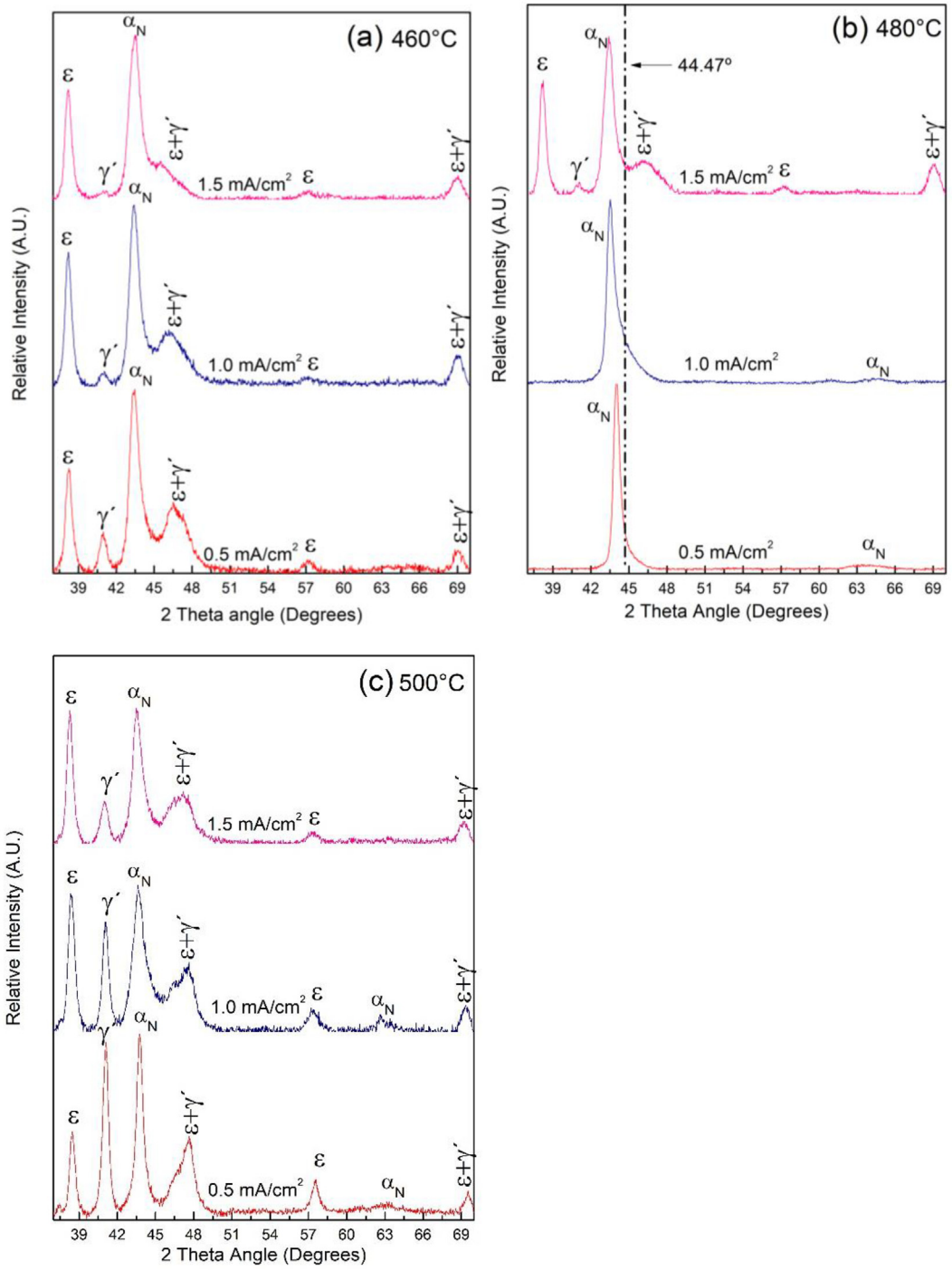

Fig. 4 – XRD pattern for plasma nitrided samples at a) 460 °C, b) 480 °C and c) 500 °C and different current densities.

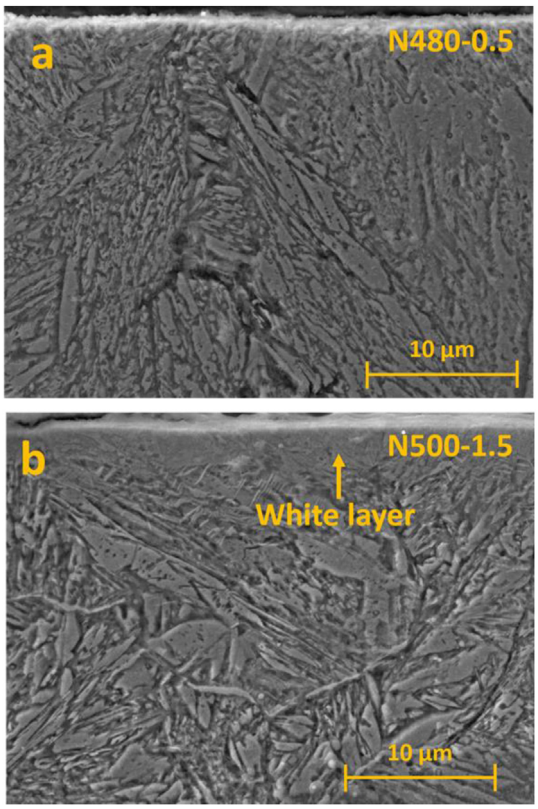

Fig. 5 – Cross SEM views for samples without (a) and with (b) presence of white layer (Nital 5%).

the expanded martensite increases, as demonstrated by the behavior in the 480–1.0 sample. This nanocrystallization phenomenon has been reported in the literature for plasma nitrided 38CrMoAl steel, where ultra-refined grains of expanded austenite, measuring approximately 10 nm, were

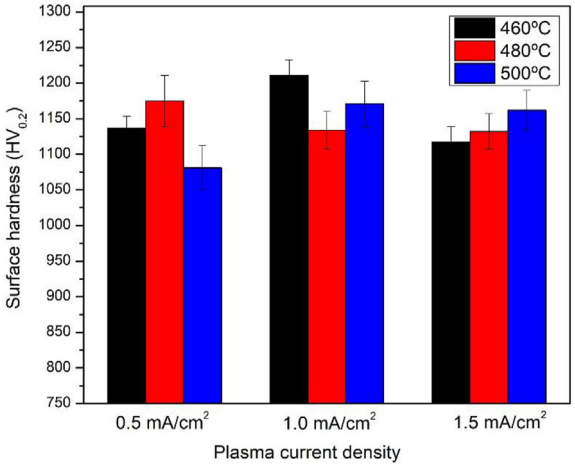

Fig. 7 – Surface hardness variation as a function of nitriding current density and temperature.

obtained, indicating high hardness, strength, and toughness for this phase [14].

3.2. *Tribological performance and nano-mechanical evaluation*

Fig. 9 illustrates the variation of the friction coefficient (CoF) with the sliding distance in the ball-on-disk test for all nitrided samples. The CoF values for samples containing the white layer (as detected in XRD) reach a steady state, exhibiting lower values (compared to the untreated sample) within the range of 2000–3000 laps. However, samples featuring an expanded martensite phase (N480–0.5 and N480–1.0) exhibit CoF values lower than those of the untreated steel throughout the test, gradually increasing towards the end until it approaches the CoF of the untreated steel. Comparable results

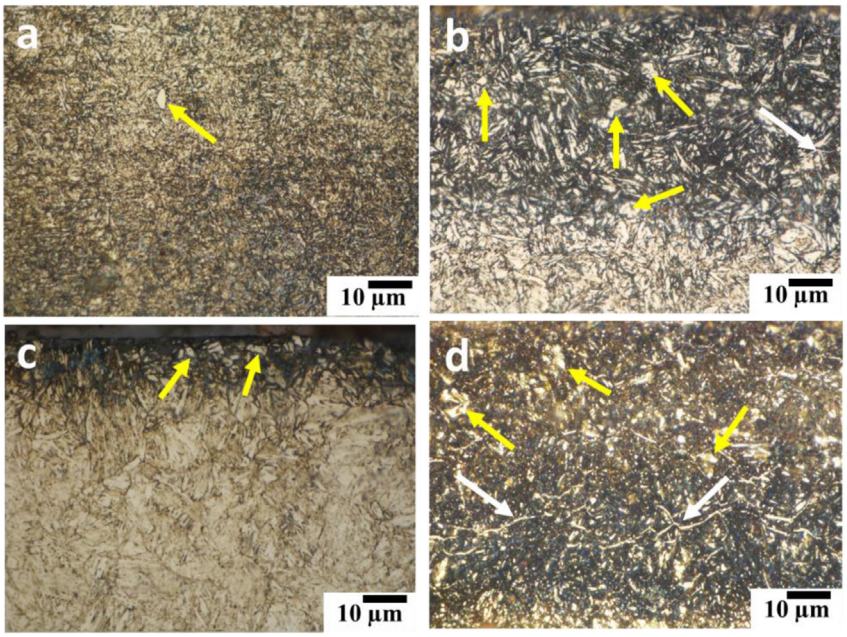

Fig. 6 – Optical micrographs of a) substrate and cross section of samples b) N460–0.5, c) N480–0.5 and d) N500–0.5.

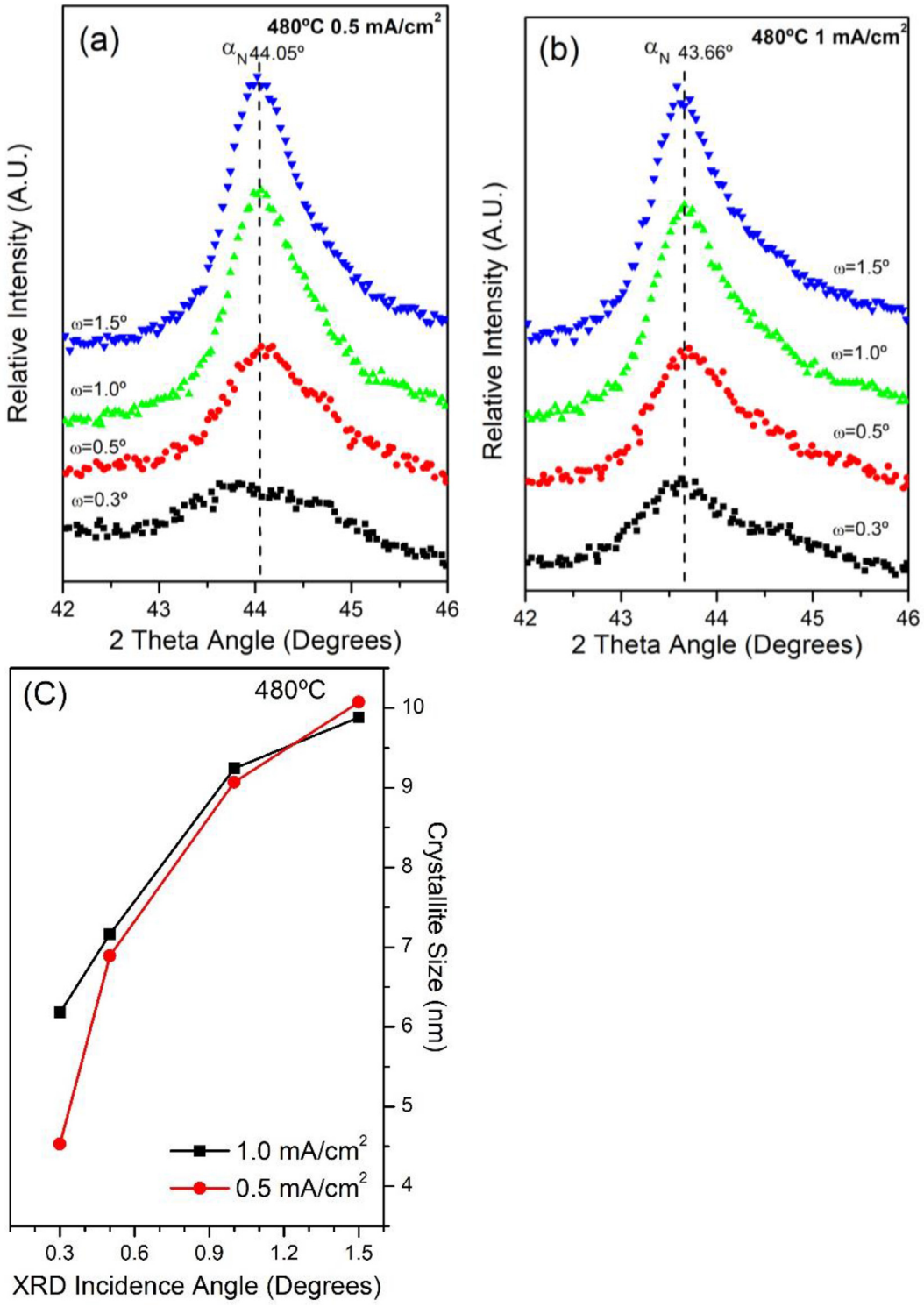

Fig. 8 – GIXRD of the main reflection of expanded martensite (110) for N480–0.5 and N480–1.0 samples and crystallite size as a function of incidence angle.

were reported in the literature for neutral nitriding of H13 steel for 3, 6, and 12 h [15]. Despite being fragile, the white layer reduces the CoF, attributed to the contact state and surface roughness. A lower contact area between the samples with a white layer (higher roughness) and the alumina ball results in a lower CoF. This phenomenon is not observed for samples without a white layer, where the contact area is higher due to lower roughness.

The wear track SEM image, along with the XRD pattern for collected debris and oxygen mapping of the untreated sample, are displayed in Fig. 10. It shows a wear track with approximately 860 μm in width. The SEM images at high

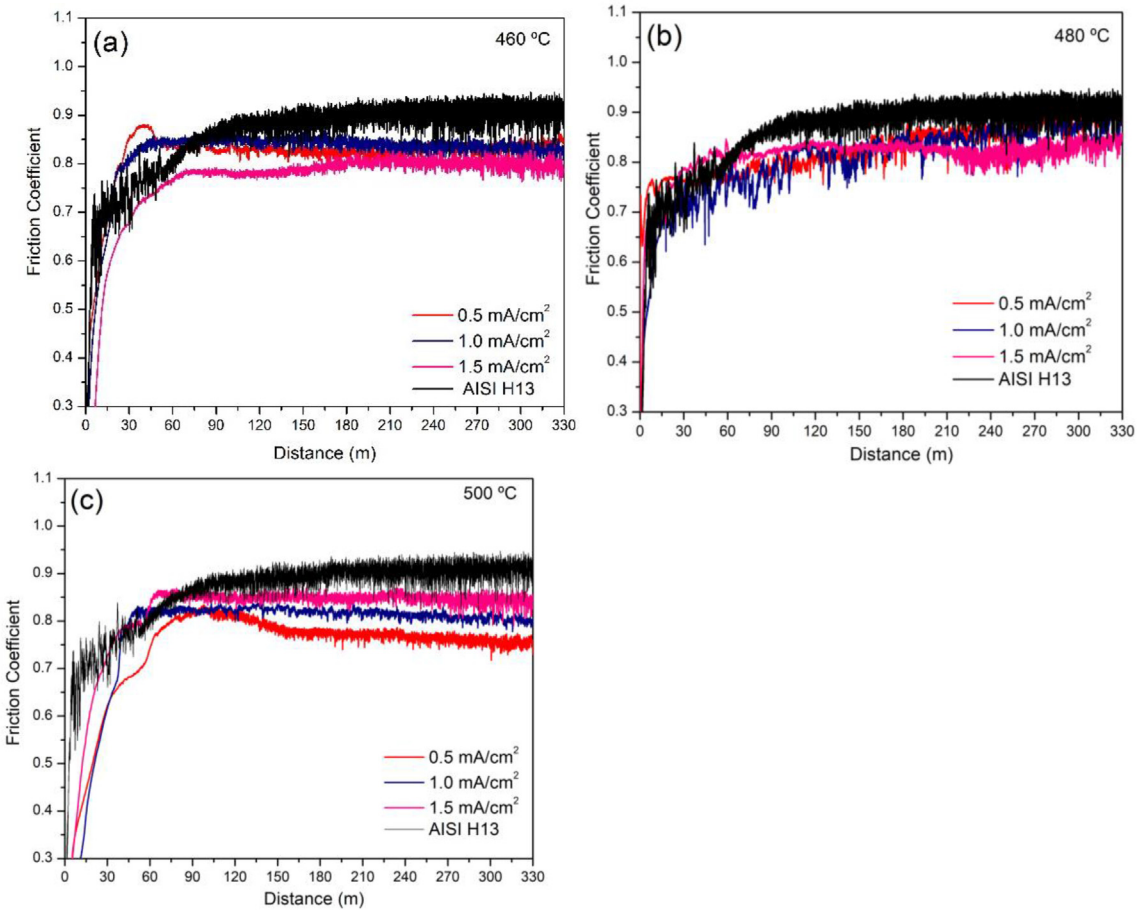

Fig. 9 – Friction coefficient as a function of distance in ball-on-disk tests for nitrided samples at different processing conditions.

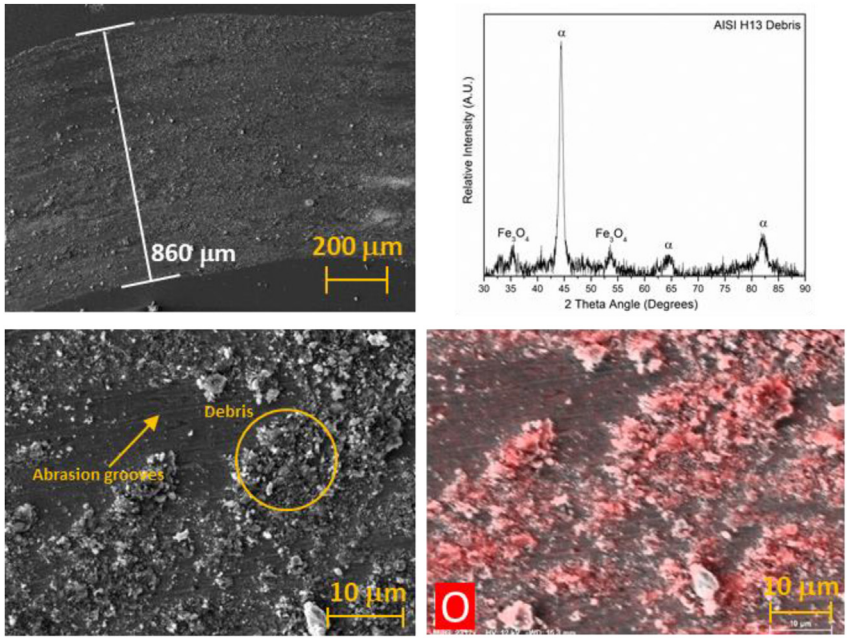

Fig. 10 – SEM surface images, XRD pattern, and oxygen mapping for wear track of untreated H13 and XRD pattern from collected debris after wear test.

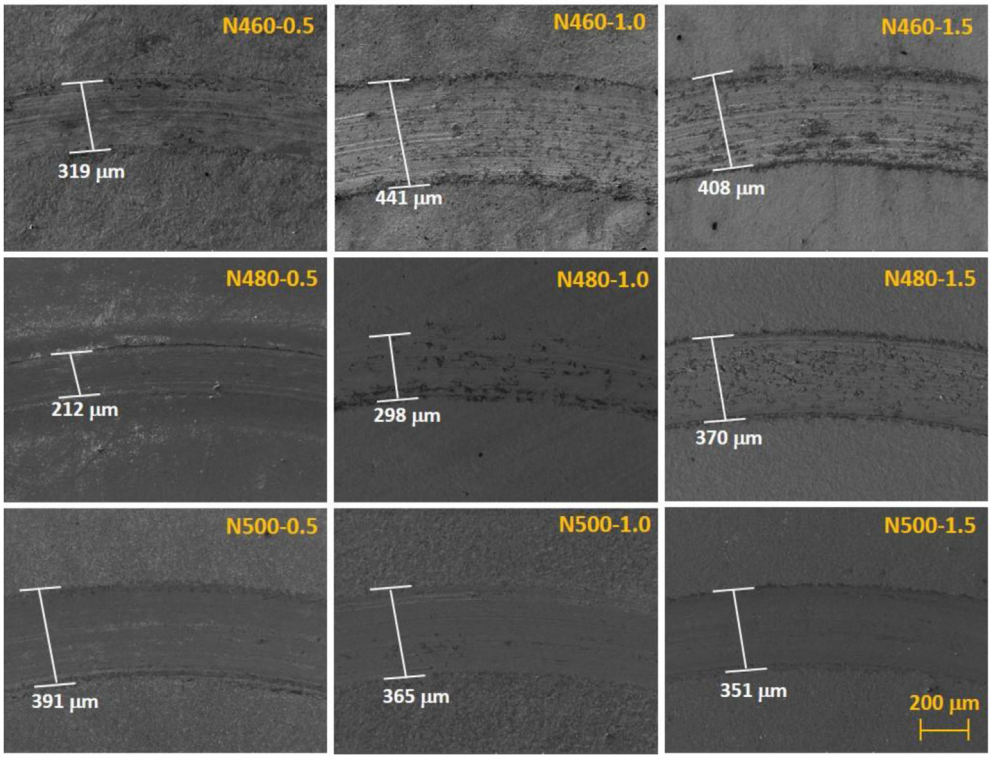

Fig. 11 – Low-magnification SEM images of wear tracks of nitrided samples.

magnification identify abrasive wear as the primary damage mechanism, with the presence of depth grooves and debris. As observed in EDS mapping, debris is oxygen-rich, while XRD analysis of collected debris validates the prominent presence of Fe_3O_4. This is the typical sliding wear performance for H13 tool steel, which has been reported previously [6].

Low-magnification SEM images of the wear tracks of nitrided samples are presented in Fig. 11. It can be observed

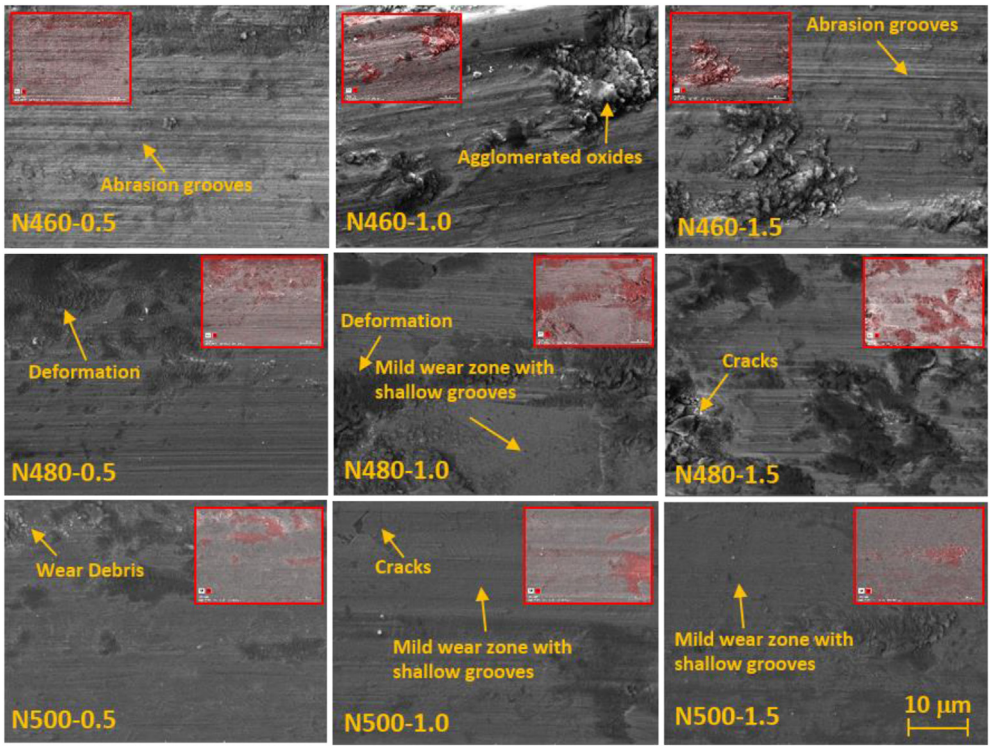

Fig. 12 – High-magnification SEM images of wear tracks of nitrided samples.

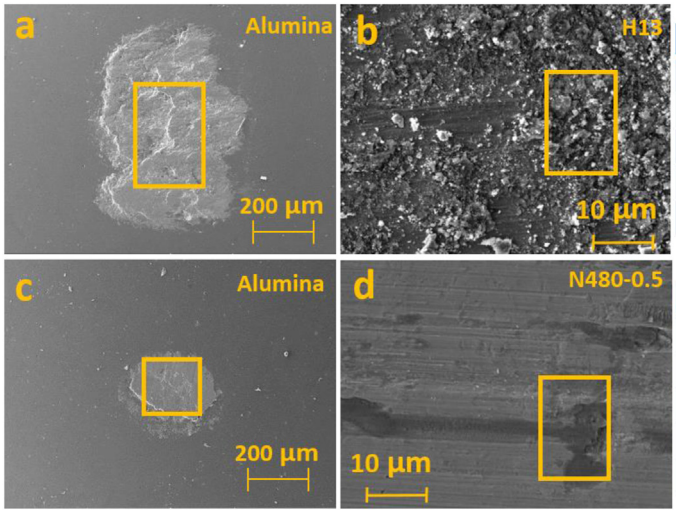

Element	Ball (%)	H13 (%)
Fe	63.21	78.5
Cr	3.25	4.86
O	24.89	14.83
Mo	--	0.98
Al	7.40	--

Element	Ball (%)	N480-0.5 (%)
Fe	75.01	82.74
Cr	4.21	2.86
O	17.53	8.39
V	--	3.31
Al	2.18	0.52

Fig. 13 – EDS analysis of wear tracks in pairs alumina ball- H13 substrate and alumina ball-N480–0.5 sample.

that the wear track width for all nitrided samples, either with or without a white layer, is narrower than that of the untreated material (see Fig. 10 (a)). For instance, the average wear track width is between 319 μm and 441 μm for samples with a white layer, whereas it is 212 μm and 298 μm for samples without a white layer (N480–0.5 and N480–1.0), respectively. In this sense, this makes evident that nitriding is improving the wear performance of the samples in comparison with the untreated one.

Fig. 12 shows SEM images with high magnification of nitrided samples wear tracks. Abrasion grooves are present in all samples, but they appear shallower for the samples processed at higher temperatures. EDS mapping indicates the presence of agglomerated oxides in all samples, suggesting an oxidative wear mechanism due to surface heating and plastic deformation [39]. A minor oxidative wear mechanism is observed in samples treated at 500 °C. The samples with a white layer display cracks due to the fragility of the layer. Finally, the samples processed at 480 °C, which only have an expanded martensite monolayer without a white layer, also exhibit mild wear zones with shallow grooves and minimal damage. Therefore, in general, plasma nitriding significantly alters the wear mechanisms compared to the untreated sample. It changes from an abrasive wear mechanism to a mechanism that involves adhesive wear, mild wear with abrasion grooves, and plastic deformation.

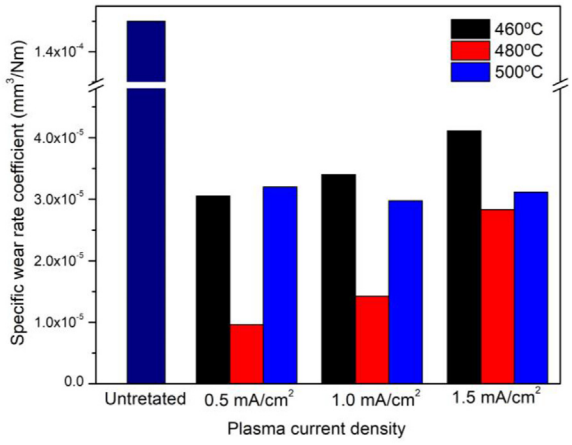

Fig. 14 – Wear rate coefficient of samples nitrided under different processing conditions.

Intending to identify the wear mechanisms in expanded martensite, Fig. 13 presents the EDS analysis of the wear tracks produced on the H13 substrate (b) and N480–0.5 samples (d), as well as the EDS analysis on their respective alumina counterparts, i.e., H13 substrate (a) and N480–0.5 (c). The relatively high content of Fe and Cr on the alumina ball confirms adhesive wear in the alumina ball-H13 substrate pair. Additionally, the track morphology and absence of Al detection in the H13 substrate track confirm the presence of mild wear with abrasion grooves and plastic deformation mechanisms. Similarly, it is evident that the wear resistance of the expanded martensite improves, as observed by the reduction in scar size on the alumina ball in the alumina ball-N480–0.5 pair. The EDS analysis for this pair reveals Fe and Cr on the ball and Al on the N480–0.5 sample track, providing further evidence of the adhesive mechanism. This mechanism, in accordance with the track morphology, is combined with the mild wear with abrasion grooves mechanism.

Fig. 14 plots the specific wear rate coefficients (k) for nitrided samples. It is observed that the samples with expanded martensite without nitrides presence on their surface exhibit lower k values. Moreover, the N480–0.5 sample displays the lowest k value (9.6×10^{-6} mm^3/Nm), which is only one-fifteenth of the k value obtained for the untreated sample (1.5×10^{-4} mm^3/Nm). Also, the N480–1.0 sample has a k value of 1.4×10^{-5} mm^3/Nm, which is approximately 10 times less than the k value for untreated H13. These results demonstrate that expanded martensite without iron nitrides or other unwanted precipitates (such as chromium nitrides) exhibits exceptional anti-wear properties. Although the k values for the nitrided samples are considerably lower than those for untreated H13 steel, samples containing iron nitrides show the worst wear resistance. This can be attributed to the fragility of the white layer [40], which typically has high hardness but promotes third-body wear effects during the wear test.

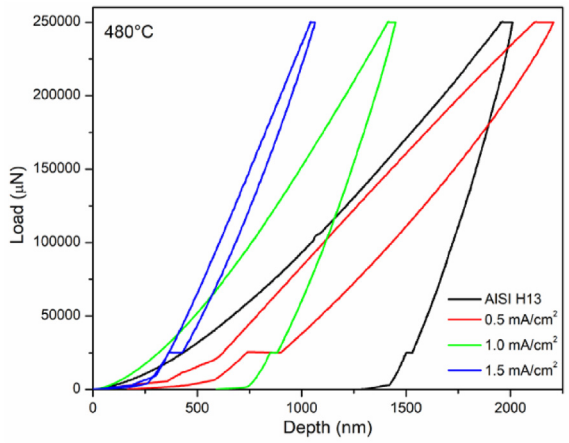

Fig. 15 – Nanoindentation curves for samples nitrided at 480 °C and different current densities.

Fig. 15 displays the nanoindentation graphs of nitrided samples at 480 °C with only expanded martensite (N480–0.5 and N480–1.0) and a white layer (N480–1.5). Additionally, Table 3 provides micromechanical information generated from the nanoindentation curves, including elastic modulus (E), nano hardness (H), micromechanical ratios H/E, H/E^2, H^3/E^2, plastic work (Wp), elastic work (We), and wear rate coefficient (k) to complement the information of the nanoindentation graphs.

Hardness to elastic module ratios (H/E, H/E^2, H^3/E^2) are essential to assess the materials mechanical performance and its deformation resistance. The H/E ratio indicates the material resistance to elastic deformation, while H/E^2 is associated with abrasive wear resistance and its ability to withstand permanent damage (i.e., plastic deformation). On the other hand, H^3/E^2 reflects the surface capacity to dissipate the plastic deformation energy when subjected to a load during a ball-on-disk test [41,42].

N480–0.5 sample, which contains expanded martensite exclusively and displays the lowest k value, exhibits the highest H/E rate (0.14) among the nitrided samples. This finding indicates the best elastic resistance of this sample. Furthermore, this sample shows the highest H/E^2 ratio (0.0058), associated with less abrasive wear damage. These ratios are consistent with the highest elastic energy value (144.5 nJ) observed for this sample, which suggests that nitriding at 480 °C and 0.5 mA/cm^2 with an expanded martensite phase leads to the best tribological performance. In contrast, the untreated H13 steel sample exhibits a plastic energy value of 133.2 nJ, indicating its performance as a rigid-plastic material. This result is due to the significantly higher E value (81.3 GPa) of the H13 steel sample compared to the N480–0.5 sample (24.2 GPa), which dissipates mostly unrecoverable energies in plastic deformation.

The nanoindentation process involves the application of an elastic-plastic load, followed by an elastic unload, which results in a displacement that represents the work done on the system (i.e., the test sample). The work manifests as heating and volumetric elastic deformation. During the unloading process, the sample does work on the nanoindenter, resulting in partial elastic recovery [43–45]. The elastic energy of expanded martensite (N480–0.5) during the unloading process is related to the H/E ratio and partially to the H/E^2 ratio. The latter is supported by the observation of the best wear performance and lower plastic deformation by the contact under a load of an alumina ball on the expanded martensite phase during the ball-on-disk test.

4. Conclusions

This work investigates the effects of temperature and current density on plasma nitriding of H13 tool steel to achieve an expanded martensite phase while avoiding the formation of an undesirable white layer. The results allow us to state the following conclusions:

Plasma nitriding at 460 °C and 500 °C leads to a modified surface composed of a mixture of ε-Fe_3N, γ-Fe_4N, and expanded martensite, regardless of the current density. Nevertheless, the content of γ-Fe_4N decreases as the current density increases from 0.5 to 1.5 mA/cm^2, which can be attributed to lower nitrogen availability at low current densities. On the other hand, an expanded martensite phase without nitrides presence can be achieved at 480 °C and current densities of 0.5 and 1.0 mA/cm^2.

GIXRD analysis shows a more disordered structure in the outer region of the nitrided zone ($\omega = 0.3°$) for expanded martensite obtained at 0.5 mA/cm^2 than at 1.0 mA/cm2. Furthermore, the sample nitrided at 480 °C and 0.5 mA/cm^2 exhibited the formation of a nanocrystallized surface with an average crystallite size of 4.53 nm.

The nitrided samples show better wear performance measured by the ball-on-disk tester over the untreated sample under all conditions. However, the sample nitrided at 480 °C and 0.5 mA/cm^2 with only expanded martensite (without white layer) shows the best wear performance ($k = 9.6 \times 10^{-6}$ mm^3/Nm). The superior wear performance of expanded martensite can be attributed to its behavior as a rigid-elastic solid with high elastic energy and strong resistance to plastic deformation, as demonstrated by the results of nanoindentation.

Declaration of competing interest

The authors declare that they have no known competing financial interests or personal relationships that could have appeared to influence the work reported in this paper.

REFERENCES

[1] Hajideh Mojtaba Rezaee, Farahani Mohammadreza. Direct laser metal deposition cladding of IN718 on DIN 1.2714 tool steel reinforced by the SiC nanoparticles. J Mater Res Technol 2023;23:2020–30.

[2] Silva Sinval Pedroso da, Mendes Abrão Alexandre, Rodrigues da Silva Ernane, Araújo Câmara Marcelo. Surface modification of AISI H13 steel by die-sinking electrical discharge machining and TiAlN coating: a promising hybrid technique to improve wear resistance. Wear 2020;(462–463):203509.

[3] Godec Matjaž, Ruiz-Zepeda Francisco, Podgornik Bojan, Donik Črtomir, Kocijan Aleksandra, Danijela A, et al. The influence of the plasma-nitriding temperature on the microstructure evolution and surface properties of additive-manufactured 18Ni300 maraging steel. Surf Coating Technol 2022;433:128089.
[4] Araújo AGF, Naeem M, Araújo LNM, Costa THC, Khan KH, Díaz-Guillén JC, et al. Design, manufacturing and plasma nitriding of AISI-M2 steel forming tool and its performance analysis. J Mater Res Technol 2020;9(6):14517–27.
[5] Miyamoto Junji, Abraha Petros. The effect of plasma nitriding treatment time on the tribological properties of the AISI H13 tool steel. Surf Coating Technol 2019;375:15–21.
[6] Díaz-Guillén JC, Alvarez-Vera M, Díaz-Guillén JA, Acevedo-Davila JL, Naeem M, Hdz-García HM, et al. A hybrid plasma treatment of H13 tool steel by combining plasma nitriding and post-oxidation. J Mater Eng Perform 2018;27:6118–26.
[7] Fernandes FAP, Heck SC, Picone CA, Casteletti LC. On the wear and corrosion of plasma nitrided AISI H13. Surf Coating Technol 2020;381:125216.
[8] Wu Jiqiang, Mao Changjun, Wei Kunxia, Hu Jing. Titanium-modified plasma nitriding layer and enhanced properties for 42CrMo steel. J Mater Res Technol 2022;18:3819–25.
[9] Alsaran Akgün. Determination of tribological properties of ion-nitrided AISI 5140 steel. Mater Char 2002;49(2):171–6.
[10] Cisquini Paula, Ramos Simão Vervloet, Viana Pedro Rupf Pereira, Lins Vanessa de Freitas Cunha, Franco Adonias Ribeiro, Vieira Estéfano Aparecido. Effect of the roughness produced by plasma nitrocarburizing on corrosion resistance of AISI 304 austenitic stainless steel. J Mater Res Technol 2019;8(2):1897–906.
[11] Che HL, Lei MK. Microstructure of perfect nitrogen-expanded austenite formed by unconstrained nitriding. Scripta Mater 2021;194:113705.
[12] Qin Xujuan, Guo Xianglong, Lu Junqiang, Chen Liangyu, Qin Jining, Lu Weijie. Erosion-wear and intergranular corrosion resistance properties of AISI 304L austenitic stainless steel after low-temperature plasma nitriding. J Alloys Compd 2017;698:1094–101.
[13] Danijela A. Skobir balantič, crtomir donik, bojan podgornik, aleksandra kocijan, matjaž godec. Improving the surface properties of additive-manufactured inconel 625 by plasma nitriding. Surf Coating Technol 2023;452:129130.
[14] Wang YX, Chen ZB, Yan MF, Zhang CS, Chen HT, Zhu YD. Preparation and characterization of ultra-refined expanded martensite α′N. Surf Coating Technol 2017;326(A):216–23.
[15] Sun Ji, Li Jie, Xie JM, Yang Yang, Wu WP, Zhou Xiang, et al. Properties of rapid arc discharge plasma nitriding of AISI 420 martensitic stainless: effect of nitriding temperatures. J Mater Res Technol 2022;19:4804–14.
[16] Yao JW, Yan FY, Yan MF, Zhang YX, Huang DM, Xu YM. The mechanism of surface nanocrystallization during plasma nitriding. Appl Surf Sci 2019;488:462–7.
[17] Pinedo Carlos Eduardo, Larrotta Sharys Ivonn Varela, Nishikawa Arthur Seiji, Dong Hanshan, Li Xiao-Ying, Magnabosco Rodrigo, et al. Low temperature active screen plasma nitriding of 17–4 PH stainless steel. Surf Coating Technol 2016;308:189–94.
[18] Espitia LA, Dong Hanshan, Li Xiao-Ying, Pinedo CE, Tschiptschin AP. Scratch test of active screen low temperature plasma nitrided AISI 410 martensitic stainless steel. Wear 2017;376–377(A):30–7.
[19] Espitia LA, Dong Hanshan, Li Xiao-Ying, Pinedo CE, Tschiptschin AP. Cavitation erosion resistance and wear mechanisms of active screen low temperature plasma nitrided AISI 410 martensitic stainless steel. Wear 2015;332–333:1070–9.
[20] Kochmański P, Długozima M, Baranowska J. Structure and properties of gas-nitrided, precipitation hardened martensitic stainless steel. Materials 2022;15(3):1–17.
[21] Yang Yang, Yan MF, Zhang SD, Guo JH, Jiang SS, Li DY. Diffusion behavior of carbon and its hardening effect on plasma carburized M50NiL steel: influences of treatment temperature and duration. Surf Coating Technol 2018;333:96–103.
[22] Dalibon Eugenia, Charadia Raúl, Cabo Amado, Sonia P, Brühl. Short time ion nitriding of AISI 420 martensitic stainless steel to improve wear and corrosion resistance. Mater Res 2019;22(6):1–8.
[23] Wang Bo, Zhao Xingfeng, Li Wenzheng, Qin Ming, Gu Jianfeng. Effect of nitrided-layer microstructure control on wear behavior of AISI H13 hot work die steel. Appl Surf Sci 2018;431:39–43.
[24] Fazel Zahra Andalibi, Hassan Elmkhah, Nouri Meisam, Fattah-alhosseini Arash. Effect of compound layer on the corrosion behavior of plasma nitrided AISI H13 tool steel. Mater Res Express 2019;6:056412.
[25] Peng Tiantian, Zhao Xiaobing, Chen Yao, Tang Lei, Wei Kunxia, Hu Jing. Improvement of stamping performance of H13 steel by compound-layer free plasma nitriding. Surf Eng 2020;36(5):492–7.
[26] Jacobsen SD, Hinrichs R, Aguzzoli C, Figueroa CA, Baumvol IJR, Vasconcellos MAZ. Influence of current density on phase formation and tribological behavior of plasma nitrided AISI H13 steel. Surf Coating Technol 2016;286:129–39.
[27] Cullity BD. Elements of X-ray diffraction. 2nd. Ed. Addison-Wesley Publishing; 1978.
[28] ASTM G99-17. Standard test method for wear testing with a pin-on-disk apparatus. ASTM International; 2017.
[29] Archard JF. Contact and rubbing of flat surfaces. J Appl Phys 1953;24(8):981–8.
[30] Zhao C, Li CX, Dong H, Bell T. Study on the active screen plasma nitriding and its nitriding mechanism. Surf Coating Technol 2006;201(6):2320–5.
[31] Roliński E, Sharp G, Arner J. Negative effects of reactive sputtering in an industrial plasma nitriding. J Mater Eng Perform 2005;14:343–50.
[32] Zhang Zhenxue, Li Xiaoying, Dong Hanshan. Plasma-nitriding and characterization of FeAl40 iron aluminide. Acta Mater 2015;86:341–51.
[33] Scheuer CJ, Zanetti FI, Cardoso RP, Brunatto SF. Ultra-low to high-temperature plasma-assisted nitriding: revisiting and going further on the martensitic stainless-steel treatment. Mater Res Express 2018;6(2):026529.
[34] Roliński E. Plasma-assisted nitriding and nitrocarburizing of steel and other ferrous alloys. In: Mittemeijer Eric J, Somers Marcel AJ, editors. Thermochemical surface engineering of steels. Woodhead Publishing; 2015. p. 413–57.
[35] Walkowicz J, Supiot P, Smolik J, Grushin M. The influence of the N2–H2 mixture composition on the spectroscopic and temporal behaviour of glow discharge characteristics in pulse-supplied nitriding processes. Surf Coating Technol 2004;180–181:407–12.
[36] Granda-Gutiérrez EE, López-Callejas R, Peña-Eguiluz R, R Valencia A, Mercado-Cabrera A, Barocio SR, et al. V-I curves and plasma parameters in a high density DC glow discharge generated by a current-source. J Phys Conf 2008;100:062019.
[37] Leite MV, Figueroa CA, Corujeira Gallo S, Rovani AC, Basso RLO, Mei PR, et al. Wear mechanisms and microstructure of pulsed plasma nitrided AISI H13 tool steel. Wear 2010;269(5–6):466–72.
[38] Canale LCF, Mesquita RA, Totten GE. Failure analysis of heat treated steel components. ASM International; 2008. p. 338–44 [Chapter 11]. Failure Analysis in Tool Steels.

[39] Straffelini G, Pellizzari M, Maines L. Effect of sliding speed and contact pressure on the oxidative wear of austempered ductile iron. Wear 2011;270(9–10):714–9.
[40] Fernández de Ara J, Almandoz E, Palacio JF, Fuentes GG, Rodríguez RJ, García JA. Influence of temperature in arc-activated plasma nitriding of maraging steel in solution annealed and aged conditions. Surf Coating Technol 2014;258:754–62.
[41] Alvarez-Vera M, Hdz-García HM, Díaz-Guillén JC, Muñoz-Arroyo R, Acevedo-Davila JL, Mtz Enriquez AI, et al. Tribological performance of Ti nanolayer coating post plasma nitriding treatment on Co based alloy. Wear 2021;477:203798.
[42] Leyland A, Matthews A. On the significance of the H/E ratio in wear control: a nanocomposite coating approach to optimised tribological behavior. Wear 2000;246(1–2):1–11.
[43] Alkorta J, Martínez–Esnaola JM, Gil Sevillano J. Comments on "Comment on the determination of mechanical properties from the energy dissipated during indentation" by J. Malzbender [J. Mater. Res. 2005;20:1090]. J Mater Res. 2006; 21; 302-305.
[44] Cheng Yang-Tse, Li Zhiyong, Cheng Che-Min. Scaling relationships for indentation measurements. Philos Mag A 2002;82(10):1821–9.
[45] Fischer-Cripps Anthony C. Nanoindentation. third ed. New York: Springer Science+Business Media; 2011.